European Conference on Computational Fluid Dynamics
ECCOMAS CFD 2006
P. Wesseling, E. Oñate, J. Périaux (Eds)

IMPROVEMENT OF DELAYED DETACHED-EDDY SIMULATION FOR LES WITH WALL MODELLING

Andrey K. Travin*, Mikhail L. Shur*, Philippe R. Spalart† and Mikhail Kh. Strelets*

* New Technologies and Services,
Dobrolyubov Ave. 14, 107198 St.-Petersburg, Russia
e-mail: strelets@mail.rcom.ru

† Boeing Commercial Airplanes
P.O. Box 3707, Seattle, WA 98124, U.S.A.
e-mail: philippe.r.spalart@boeing.com

Key words: Detached-Eddy Simulation, Large Eddy Simulation, Wall-Modeling LES

Abstract. *Adjustments are proposed of the Delayed Detached Eddy Simulation (DDES) approach to turbulence. They preserve the DDES capabilities particularly for natural DES uses, and resolve the mismatch of the logarithmic layers discovered earlier for the basic DES technique when used for Wall-Modelled Large-Eddy Simulation (WMLES) of attached flows. The adjustments are defined both for the Spalart-Allmaras and the Menter SST models. The first one concerns the definition of the LES length scale in general for anisotropic grids near a wall, and makes use of the wall distance along with the grid spacing; it clearly benefits even the Smagorinsky model. The second one manages the blending of RANS and LES behaviour within a WMLES to advantage, greatly increasing the resolved turbulence activity near the wall, and finely adjusting the resolved logarithmic layer. This is seen in channel flow over a wide Reynolds-number range, and through some grid variations. Tests show that the new method, although somewhat more complex, returns the desired behaviour not only in channel-flow LES, but also in channel-flow RANS, in a backward-facing-step case with side-by-side LES and RANS regions, and over an airfoil in deep stall.*

1 INTRODUCTION

The importance of the problem of Wall Modelling in LES has motivated numerous studies, and some rather complex proposals. Many of them use substantial outside information such as fields from well-resolved LES or DNS runs (e.g., Davidson and Dahlstrom[1)]) or synthetic turbulence (e.g., Davidson and Billson[2)]) at the RANS-LES interface, and/or require averages in the wall-parallel directions to define intermediate quantities (e.g., Temmerman *et al.*[3)]) or to avoid negative eddy viscosities and similar difficulties. Although rather successful in the simple flows, these proposed solutions become very debatable once a complex geometry is involved. In contrast to this, no impractical, "channel-friendly" steps are needed when DES is used for wall modelling in LES. The equations of DES provide a simple and robust "wall model" for LES, and since the problem of wall modelling is arguably the principal one for LES, building from the DES equations could be a very viable way to empower LES principally in terms of Reynolds number.

It is quite generally recognized that wall modelling naturally uses RANS logic near the wall, in the region where the wall distance is much smaller than the boundary-layer thickness, but very large in wall units, and the grid spacings parallel to the wall are also very large in wall units. The averaging is not over infinite spatial or temporal samples, but over samples large compared with the scales of the turbulence at the present distance from the wall. Therefore, the fact that DES contains RANS empiricism does not make DES-based methods any less fundamental than the other ones. Note that DES and similar approaches that draw both on Reynolds-Averaged Navier-Stokes (RANS) models and on LES have uses that may be called "natural," and other uses which are described as "extended", but are equally promising. A natural tendency in such situations is to optimise a version of the approach for each of the uses, but this is not desirable here. The ambition is to have a single set of formulas, so that different regions inside a single simulation over a complex geometry can benefit from different modes.

Natural DES uses treat the boundary layers with RANS, and the massively-separated regions with LES. Extended uses treat even attached boundary layers and other wall-bounded flows with LES, i.e., are essentially WMLES approaches; most of the exercises have actually been conducted in channels. This defeats the initial purpose of DES, namely avoiding the high cost of LES in relatively simple boundary layers, if it is applied over the entire domain; thus, any sensible practical application will confine LES to regions of very thick boundary layer, and still treat the thin boundary layers with RANS. This will be achieved by proper grid design, and be assisted by the DDES correction[5]. Another view is that the initial or natural concept of DES is aimed at external aerodynamic flows, and that many internal flows have different needs: the flow region is filled with turbulence. The descriptions "natural" and "extended" could, therefore, be supplemented by words such as "external-flow priority" and "internal-flow priority."

The first attempt at a DES application as WMLES in the study of Nikitin *et al*.[4] was overall successful, in that very large grid spacings, in wall units, were used without trouble and the response to grid refinement and Reynolds-number variations was spotless. However two issues remained.

The first is that the wall-normal grid spacing is not large in wall units, with a typical value of 1 for the first point, as is normal in RANS practice without wall functions. Some in the community consider that even the wall-normal spacing should be unlimited in wall units; roughly, the near-wall grid cells could be cubic just like the cells away from the wall. This might be achieved some day, but the extra difficulty is substantial, and the practical value of it would be limited by the fact that, with grid stretching, the grid count increases only logarithmically with Reynolds number even as the first spacing drops almost as fast as the inverse of that number. In other words, the cost of being limited to $y^+ \sim 1$ is very manageable.

The second issue, which has received more attention, is the "Log-Layer Mismatch" or LLM. As expected, the channel simulations produced two stacked logarithmic layers, once the resolution and Reynolds number were sufficient. The lower one, the modeled log-layer, arises because the RANS model was constructed to provide it. The upper or resolved log-layer arises

because LES is functioning well once all three grid sizes are much smaller than the distance to the wall. The Karman constants of the two layers are close (not that the grids were fine enough to discuss the exact value of κ). The mismatch is in the level of the two log-layers, or intercept, C. The resolved layer has a higher C by almost 3 units, which is substantial, as it lowers the skin-friction coefficient by 15 to 20%. It must be emphasized again that a realistic set of expectations for WMLES by the DES equations with no adjustment at all, as used by Nikitin *et al*.[4], would not have included a good match of the two log-layers. The nature of the simulation changes completely across an ambiguous region, from the turbulence being fully modeled to it being almost fully resolved, which prevents any genuine connection between the two layers. Therefore a solution to LLM, which is the goal of the present work, is very unlikely without adding empiricism, essentially aimed at a single result: the intercept of the resolved log layer. Note that LES Sub-Grid-Stress (SGS) and especially wall models in the literature all contain much empiricism, and some are limited in terms of grid aspect ratios and similar respects. The challenge is to repair LLM in DES without hurting its accuracy in other regions, and with as little extra complexity as possible.

Another goal, more qualitative, is to "make good use" of the grid; visualizations showed that the smallest resolved eddies are commensurate with the grid in center of the channel, but not near the wall, where the eddies are very elongated and slowly-evolving. There is a distinct impression that the resolution is wasted, which is rarely good; even if LLM were absent in the channel, other flows with some streamwise gradients of the boundary conditions and mean flow would have to benefit from a decent use of the grid spacing.

This present work starts from DDES, which will be in print very soon[5] and will become the standard version of DES, barring unforeseen problems as it starts being used outside the originator group. DDES is opposed to the original version[6], now called DES97. The difference is that DDES handles "ambiguous" grids much better than DES97. Such grids, fine enough to activate the DES limiter on eddy viscosity but not to support an accurate LES, confuse DES97[5-7]; in contrast, DDES detects such situations and quite reliably keeps the model in RANS mode. This is at the price of a moderate increase in complexity, and also of new behaviours including the higher likelihood of multiple solutions. Therefore, it is important to detect possible disruptive interference between DDES and the new changes proposed here, but these changes will work with both versions of DES.

The rest of the paper is organized as follows. In Section 2 we present the new model formulation which includes a subgrid length-scale definition (2.1) and a detailed description of the suggested RANS-LES hybridization (2.2). Then, in Section 3 a series of model tests is presented which includes its application to channel flow over a wide Reynolds-number range, i.e., in a pure WMLES mode, to a backward-facing-step flow with side-by-side LES and RANS regions, and, finally, to an airfoil in deep stall, i.e., in the "natural" DES mode.

2 MODEL FORMULATION

The modifications to DDES suggested in the present work to resolve the LLM issue are fairly minor in terms of implementation, but not as minor in theoretical terms. The two major elements are: a new definition of the subgrid length-scale that includes an explicit

wall-distance dependence, unlike the usual LES practice which involves only the grid spacing, and an empirical RANS-LES hybrid function designed to provide a more successful coupling of the two approaches inside attached boundary layers. The presentation assumes a structured orthogonal grid, so that the wall-parallel spacings are uniform.

2.1 Subgrid length-scale definition

The issue of the adequate definition of the subgrid length-scale in an LES is far from trivial, especially when the computational grid is significantly anisotropic, which is typical of the wall-bounded flows we are concerned with in the present study. Almost all simulations of such flows use a finer spacing in the wall-normal direction than in the other two directions, and some also use finer spacing in the lateral direction than in the streamwise direction. Historically, the most widely employed definition has been the cubic root of the cell volume. While this is a plausible balanced quantity, it was challenged in DES literature[6], in which the maximum of the three cell dimensions was advocated instead. Neither definition is successful, if judged by a straightforward application to well-resolved LES of wall-bounded flows: the SGS constants which work well in free turbulent flows with cubic cells are then too large. For instance, the optimal value of the Smagorinsky constant for LES of channel flow is about 0.1 if the cube root is used, or roughly half its optimal value for Decaying Isotropic Homogeneous Turbulence (DIHT). Using the maximum grid spacing as in DES97[6] and DDES[5], the difference between the optimal model constants for DIHT and channel flows is even larger. This suggests that neither choice of the subgrid length-scale is successful, and motivates a search for another, more physically justified, definition which would not demand an adjustment of the subgrid model constants for LES of different turbulent flows.

Since wall-proximity effects, primarily inviscid blocking, are involved, it seems natural to allow such a definition to rely not only on the cell sizes, but also to explicitly include a wall-distance dependency, i.e., have the form:

$$\Delta = f(h_x, h_y, h_z, d_w), \tag{1}$$

where Δ is the needed subgrid length-scale, h_x, h_y, and h_z are the local streamwise, wall-normal, and lateral cell sizes respectively, and d_w is the distance to the wall.

Let Δ_{free} be the infinite-d_w limit of the function $f(h_x, h_y, h_z, d_w)$. Then, following the concept in the DES papers (recall, however, that this is a general LES issue), it is set equal to the maximum local grid spacing

$$\Delta_{free} = h_{\max} \equiv \max\{h_x, h_y, h_z\}. \tag{2}$$

Note that away from the walls, the grid for an LES should be fairly isotropic anyway, and so the impact of this specific choice is not crucial.

As for the behaviour of Δ in close vicinity of the wall, it should not follow the drastic decrease of the wall-normal step typical of this region and, therefore, should depend on the wall-parallel steps only:

$$\Delta_{wall} = const(d_w) = \Delta(h_x, h_z) \tag{3}$$

Assuming, finally, that between these two limiting cases Δ is a linear function of d_w and that at any distance to the wall it varies within the range $h_{\min} \le \Delta \le h_{\max}$, a definition of the subgrid length-scale satisfying all the above demands is formulated as follows:

$$\Delta = \min\{\max[C_w d_w, C_w h_{\max}, h_{wn}], h_{\max}\}, \tag{4}$$

where h_{wn} is the grid step in the wall-normal direction and C_w is an empirical constant set equal to 0.15 based on a well-resolved LES of the developed channel flow, as seen shortly.

Figure 1 shows two possible types of variation of the subgrid length-scale Δ defined by (4), normalized by the maximum grid step, across a plane channel with half-width H.

The first type (solid line in Fig.1) takes place if $h_{wn} \le C_w d_w$ and, therefore, in accordance with (4), as long as $d_w < h_{\max}$, the length scale Δ remains constant equal to $C_w h_{\max}$. Then, once $d_w > h_{\max}$, it grows linearly ($\Delta = C_w d_w$) until reaching the value of $h_{\max}$, and stays constant after that.

The second type of Δ variation (dashed line in Fig.1) corresponds to a strong wall-normal step stretching. In this case, Δ remains constant equal to $C_w h_{\max}$ as long as $h_{wn} < C_w h_{\max}$. Then, it grows with a rate higher than C_w until reaching the value of $h_{\max}$ and after that, just as in the first case, remains constant. Note that this scenario is undesirable, but still is not a disaster. For instance, for a wall-normal step varying in accordance with a geometric series, it takes place if $k > (1 + C_w) = 1.15$, which is acceptable. On the other hand, the value of k for a sufficiently accurate LES should not be larger than $1.2 \div 1.3$.

An example illustrating the performance of the subgrid length-scale (4) in the framework of a well-resolved LES with the use of the Smagorinsky model is presented in the next section.

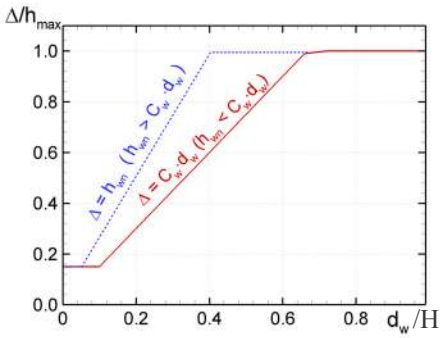

Figure 1: Two typical types of variation of the subgrid length-scale (4) across the plane channel

2.2 RANS-LES hybridization

Here the model couples the two approaches via introduction of a hybrid turbulent length-scale based on the following blending of the RANS and LES length-scales:

$$\widetilde{l} = f_{hyb}(1 + f_{restore}\Psi)l_{RANS} + (1 - f_{hyb})C_{DES}\Psi\Delta, \tag{5}$$

where Δ is the subgrid length-scale defined by (4) and C_{DES} is the empirical constant of the LES branch of DES[6, 8].

In accordance with the general DES concept[6, 9, 10], in order to create a hybrid model, the hybrid length-scale $\widetilde{l}$ defined by (5) will be substituted into the background RANS model in place of the RANS length scale, l_{RANS}, explicitly or implicitly involved in any such model. For instance, for the Spalart-Allmaras model[11] (SA model), the length scale is equal to the distance to the wall $l_{RANS} = d_w$ while for the $k-\omega$ SST model of Menter[12] (MSST model), $l_{RANS} = k^{1/2}/(C_\mu\omega)$.

Let us now consider the ingredients of the hybrid length scale (5) in more detail.

The hybrid function f_{hyb} includes DDES and WMLES branches and reads as:

$$f_{hyb} = \max\{(1 - f_d), f_{step}\}, \tag{6}$$

Here the function f_d is the delay function of DDES[5]

$$f_d = 1 - \tanh[(8r_d)^3],\ r_d = \frac{1}{\kappa^2 d_w^2}\cdot\frac{\nu_t}{\max\{[(\partial u_i/\partial x_j)(\partial u_i/\partial x_j)]^{1/2}, 10^{-10}\}} \tag{7}$$

and the function f_{step}, which is active only when the model operates in WMLES mode, provides a rapid switch from RANS to LES deep inside the boundary layer. This function is designed as follows:

$$f_{step} = \min\{2\exp(-9\alpha^2), 1.0\} \tag{8}$$

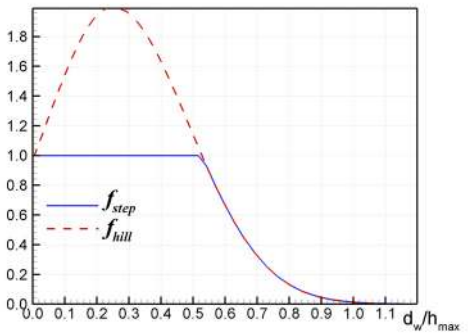

Figure: 2. Profiles of the functions f_{step} and f_{hill} in the plane channel

With the parameter α set equal to $(0.25 - d_w / h_{\max})$, f_{step} as defined by (8) provides a fast switching of the model from pure RANS to pure LES mode within the range of wall-distance $0.5h_{\max} < d_w < h_{\max}$ (see the solid blue line in Fig.2).

The positive function $f_{restore}$ involved in the definition of the hybrid length scale (5) is aimed at preventing an excessive damping of the RANS Reynolds stresses as could be caused by the interaction of the RANS and LES regions in the vicinity of their interface. Similar to the function f_{step}, this function must be active only when the hybrid model operates in WMLES mode, i.e., it has to be close to zero in two limits:

1) if the grid used in the simulation is sufficient for a well-resolved LES (a switch to LES mode occurs at $y^+ < 15 \div 20$);
2) if the hybrid model effectively performs as the background RANS model (otherwise, the activation of the function would corrupt the correct RANS behaviour).

The function built to satisfy these demands reads as:

$$f_{restore} = \max\{(f_{hill} - 1),\ 0\} f_{amp}\,. \tag{9}$$

Here the function f_{hill} shown by the dashed red line in Fig.2 together with the function f_{step} (8) reads as

$$f_{hill} = \begin{cases} 2\exp(-11.09\alpha^2) & if \quad \alpha \geq 0 \\ 2\exp(-9.0\alpha^2) & if \quad \alpha < 0 \end{cases}. \tag{10}$$

and, as seen in Fig.2, coincides with f_{step} when $f_{step} < 1$, i.e. in the transitional, RANS-LES, region.

The second function, f_{amp}, involved in (9) is defined as follows:

$$f_{amp} = 1.0 - \max\{f_t, f_l\}, \tag{11}$$

where

$$f_t = \tanh[(c_t^2 r_d)^3],\ f_l = \tanh[(c_l^2 r_{dl})^{10}], \tag{12}$$

the quantity

$$r_{dl} = \frac{1}{\kappa^2 d_w^2} \cdot \frac{\nu}{\max\{[(\partial u_i / \partial x_j)(\partial u_i / \partial x_j)]^{1/2}, 10^{-10}\}} \tag{13}$$

is a laminar analogue of the parameter r_d in (7), and c_l and c_t are additional model constants.

As seen from (10) and Fig.2, the function f_{hill} provides a "predefined" (depending on the grid but not on the solution) "restoring" device for the RANS branch of the hybrid model

length-scale (5). In contrast, the "amplitude" function f_{amp} (11) controls the "restoring intensity" through the parameters r_d and r_{dl} which depend on the solution. Such distinctions have become familiar starting with DDES. The constants c_l and c_t depend on the background RANS turbulence model and are adjusted so that the function is virtually zero when either r_{dl} or r_d is close to 1. Considering that r_{dl} is close to 1 in the laminar sublayer and r_d is close to 1 in the logarithmic part of the turbulent boundary layer computed by RANS[11], the function f_{amp} and, therefore, $f_{restore}$ is made close to zero in these two situations. As a result, both demands 1) and 2) formulated above are satisfied. Based on the simulations of channel flow considered in the next section, the values of the constants c_l and c_t are set equal to 3.55 and 1.63 for the SA-based hybrid model and 5.0 and 1.87 for the MSST-based one.

The last function involved in the hybrid length-scale definition (5) is the low-Reynolds number correction Ψ from the DDES model which is introduced there in order to compensate the activation of the low-Reynolds number terms of the background RANS model in the LES mode (see Spalart *et al.*[5] for detail). In the considered hybrid model (5), in addition to that, the function Ψ provides also an amplification of the effect of $f_{restore}$ in the RANS region. Just as the constants c_l and c_t, the function Ψ depends on the background RANS model. In particular, it is equal to 1.0 for the MSST-based model which does not include any low-Reynolds number terms and for the SA-based model it is defined as follows[5]:

$$\Psi^2 = \min\left[10^2, \frac{1-\dfrac{c_{b1}}{c_{w1}\kappa^2 f_w^*}\left[f_{t2}+(1-f_{t2})f_{v2}\right]}{f_{v1}\max(10^{-10},\,1-f_{t2})}\right], \tag{14}$$

where all the notations, except for the quantity f_w^* are the same as in the SA RANS model and $f_w^* = 0.424$ [5].

3 MODEL TESTS

3.1 Overview

In this section we present results of the new hybrid model testing.

First, an example is given of the application of the new subgrid length-scale (4) for a well-resolved LES of the developed flow in a plane channel with the use of the Smagorinsky subgrid model. This example is aimed at supporting the claim that with this length-scale there is no need to change the Smagorinsky constant value calibrated based on the DIHT flow, when carrying out LES of wall-bounded flows.

Then a series of tests is presented aimed at demonstrating the capabilities of the hybrid RANS-LES models based on the hybrid length-scale (5) and SA and MSST RANS models as the background ones. In order to demonstrate the WMLES capabilities of these models, they are applied to the developed plane channel flow, which is a conventional test case for any WMLES approach. Then, the backward-facing step flow of Vogel and Eaton[13] is considered, which permits to evaluate the models' performance in a mixed, DDES-WMLES, mode. Finally, the models are applied to the flow past the NACA 0021 airfoil at 60 degrees angle of attack studied experimentally by Swalwell[14]. This is an example of the "natural DES flows", i.e., those with massive separation, DES97 and DDES are designed for. The goal of this test is to make sure that for such flows the new hybrid models are at least not less accurate than the corresponding DDES models.

All the simulations are carried out with the use of the incompressible branch of the NTS code[10]. It uses the Rogers-Kwak[15] implicit scheme. Time-derivatives are approximated with 2nd-order backward differences (three-layer scheme) with dual time-stepping (infinite default pseudo-time step) and subiterations. The number of subiterations at each time step depends on the problem being solved but usually is within the range from 5 to 20 (this ensures the reduction of the maximum residual by 3-4 orders of magnitude). Time integration is performed with the use of Gauss-Seidel relaxation by planes. For the spatial approximation of the inviscid fluxes, the code provides different options. In this work we used 4th-order centred approximation for the channel flow and hybrid, weighted 5th order upwind/4th order centred, scheme with a blending function dependent on the solution[10, 16] in all the other cases. The viscous terms in the equations are approximated with the 2nd-order centred scheme.

3.2 Well-resolved LES of plane channel flow

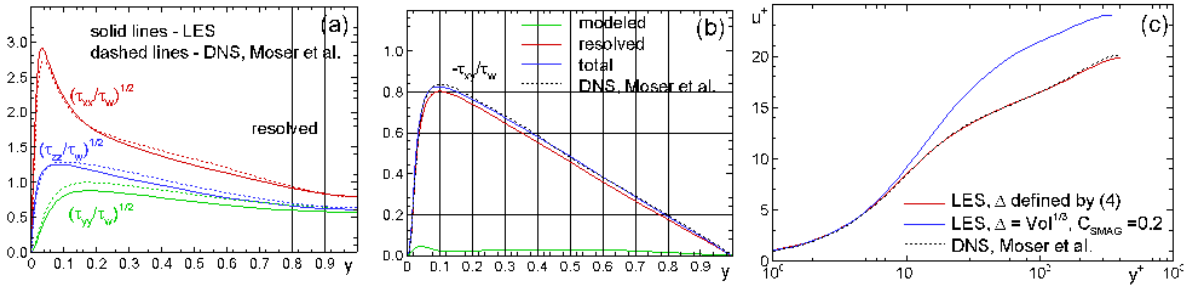

Figure 3: Resolved and modeled stresses (a), (b) and mean velocity profiles (c) from well-resolved Smagorinsky LES of developed channel flow with subgrid length-scale defined by (4) and as a cube root of the cell volume (blue curve in frame c)

Figure 3 shows results of LES of channel flow at Re_τ=400 performed with use of the Smagorinsky model with the wall-damping function[17]:

$$\nu_t = (C_{SMAG}\Delta)^2 \{1 - \exp[-(y^+/25)^3]\} S\,, \tag{15}$$

where S is the magnitude of the strain tensor, Δ is defined by (4), and C_{SMAG}=0.2 (this value was established based on LES of DIHT flow with the use of NTS code, with the objective of

maintaining a -5/3 spectral slope near the cut-off). The grid used in the simulation is as follows: $\Delta x/H = 0.1$, $\Delta z/H = 0.05$, ($\Delta_x^+ = 40$, $\Delta_z^+ = 20$), the near-wall y-step is $\Delta y_1/H = 2\times10^{-3}$ (Δy_1^+=0.8), and the stretching factor of the wall-normal step is $k = 1.14$. The size of the computational domain is $L_x = 8H$, $L_z = 3H$. The time step is 0.57, in wall units.

One can see that with the subgrid length-scale (4), results of LES agree with the DNS data of Moser *et al*.[18] very well. Thus, the test confirms that the subgrid length-scale definition (4) gives quite an accurate prediction of channel flow with the value of the Smagorinsky constant defined based on the DIHT flow. In contrast to this, with the traditional definitions via the cubic root of the cell volume or maximum grid-spacing, this results in a completely wrong solution (see blue curve in Fig.3c).

3.3 Hybrid models testing in plane channel flow

This test is, in fact, the key one, since it is aimed at the evaluation of the new models' performance as applied to attached flows, i.e., those which neither the original DES97 nor DDES, in a derivative use as wall model in LES, is capable of predicting to the level of accuracy expected in simple flows nowadays.

The series of simulations performed includes a Re_τ variation in the range from 400 up to 18000, with the use of the SA- and MSST-based versions of the hybrid model (5). The computational domain and the grid in the wall-parallel directions used in these simulations are the same as those used for the well-resolved Smagorinsky LES at Re_τ=400 considered in the previous section. Thus, the series allows an assessment of the WMLES capability of the models on grids unlimited in the sense of wall-parallel grid steps in wall units, Δx^+ and Δz^+. The wall-normal grid is built in a conventional manner. In particular, the near-wall step is adjusted to the Reynolds number, to provide a value of y_1^+ below 1.0. Then, the grid step increases with the stretch-factor 1.14. In accordance with (4), with this wall-normal step distribution, the first type of variation of the subgrid length-scale Δ across the channel (the solid line in Fig.1) takes place. The simulations are carried out with the use of the central-difference fourth order approximation of the inviscid fluxes.

Below we first present results of the simulations obtained with the use of the MSST- and then with the SA-based versions of the hybrid model (5).

MSST-based version of the hybrid model. As already mentioned, for attached flows, the outcome of simulations with the proposed hybrid models depends on whether the flow does or does not have turbulent content, which may be introduced by the initial conditions or "generated" somehow upstream of the region of interest. Let us first consider the first (with turbulent content) scenario which has been implemented via initialisation of the simulations by prescribing the flow-fields obtained from LES of the DIHT flow with the use of the subgrid version of the MSST model[10, 16] as described in[19].

Figure 4 shows profiles of the functions f_{hyb}, $(1-f_d)$, and f_{step} obtained in this case at different Re_τ (in this figure and thereafter y denotes the wall-normal coordinate normalised

with H). One can see that at the low and moderate Re_τ, $f_{step} > (1 - f_d)$ and therefore in accordance with (6) the f_{step}-branch of f_{hyb} controls the switch of the hybrid model from the RANS mode, $\tilde{l} = (1 + f_{resore}) l_{RANS}$, to the LES mode, $\tilde{l} = C_{DES}\Delta$ (as mentioned in Section 2.2, for the MSST-based version of the model, the function Ψ is equal to 1). At Re_τ=18000, both branches of f_{hyb} are active, the $(1 - f_d)$-branch prevailing near the wall and the f_{step}-one dominating in the outer part of the RANS region.

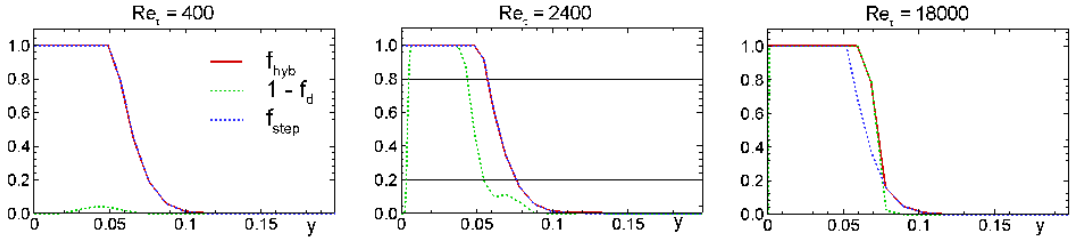

Figure 4: Profiles of the functions f_{hyb}, $(1 - f_d)$, and f_{step} in the developed channel flow at different Re_τ from the simulations with the use of the MSST-based hybrid model (5) and presence of initial turbulence content

As far as the behaviour of the restoring function $f_{restore}$ is concerned, as seen in Fig.5a, it deviates from zero only in the pure RANS region, the deviation being most pronounced at moderate Re_τ. Thus, exactly at these conditions, a strengthening of the RANS mode of the model is ensured. This is seen from Fig.5b, where profiles are plotted of the ratio of the hybrid and RANS turbulent lengths-scales, $\tilde{l} / l_{RANS}$. Consistently with the behaviour of $f_{restore}$, the ratio is higher than 1.0 in the outer part of the RANS region (see Fig.4) and is maximal at Re_τ=1100. This means a decreased level of turbulence dissipation relative to the original RANS model, which prevents too strong a decrease of the eddy viscosity in this region. In turn, this helps prevent the unwanted rise of the modelled logarithmic layer[4] which prompted the present effort. Then, in the LES region, the ratio drops rather abruptly, reaches a local minimum, and after that stays nearly constant equal to 0.6. This fast drop of the hybrid length-scale is a characteristic feature of the proposed hybrid model (in DES97 and DDES it decreases more slowly), which makes its performance in WMLES mode quite different from these models. In particular, this results in a fast decrease of the eddy viscosity which, in turn, helps to unlock the flow instabilities.

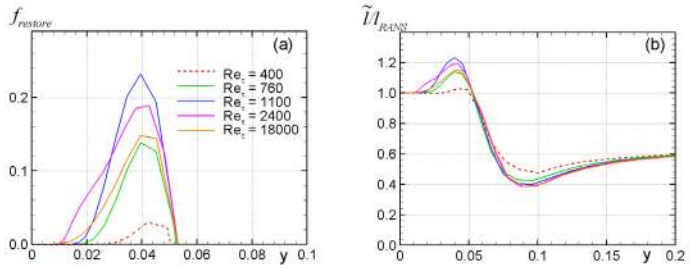

Figure 5: Profiles of function $f_{restore}$ (a) and ratio of length scales of MSST-based hybrid model (5) and MSST RANS model (b) in the channel flow at different Re_τ

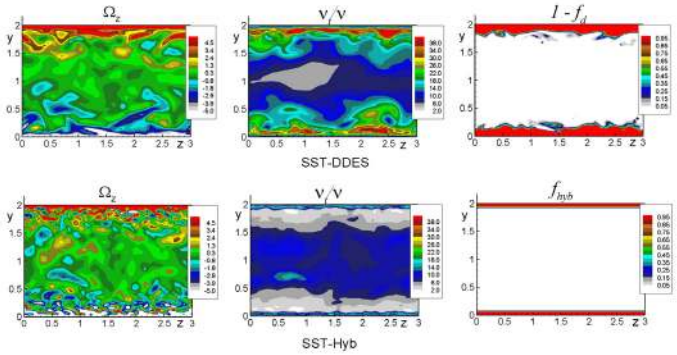

Figure 6: *YZ*-cuts of instantaneous vorticity magnitude, eddy viscosity, and hybrid function from the simulation of the developed channel flow with the MSST-based hybrid model at two Reynolds numbers

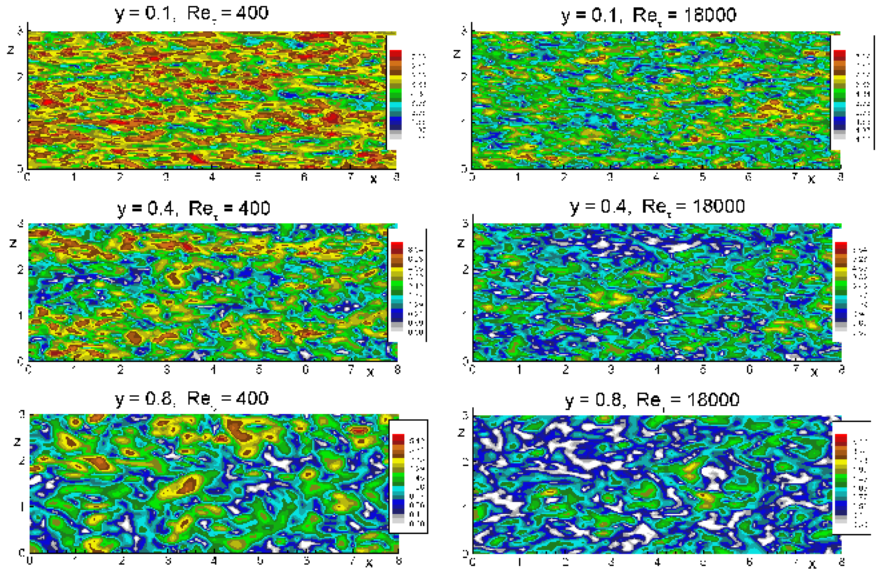

Figure 7: *XZ*-cuts of vorticity magnitude at different wall-distances from the simulation of channel flow with the MSST-based hybrid model at two Reynolds numbers

This is supported by Figs. 6, 7, where we present flow visualisations from the simulations at the lowest and highest of the considered Re_τ. The visualisations show that the hybrid model does capture the major known features of the turbulence in the channel reasonably well. In particular, the model provided a good use of the 80-by-60 grid (see the *XZ* cuts in Fig.7) and does not cause formation of smooth nearly one-dimensional eddies and excessive damping of turbulence at the RANS-LES interface, the way DES97 or DDES do[20]. These advantages of the new model are clearly seen in a direct comparison of the flow visualizations from the simulations with the use of this model and standard MSST DDES presented in Figs.8, 9. The latter model fails, specifically, near the wall, whereas the two behave very similarly near the centre of the channel. Note also that the *YZ*-cuts of the eddy viscosity obtained with a hybrid model (Figs.6, 8) reveal its steep gradients, which create vorticity and excite the near-wall layer.

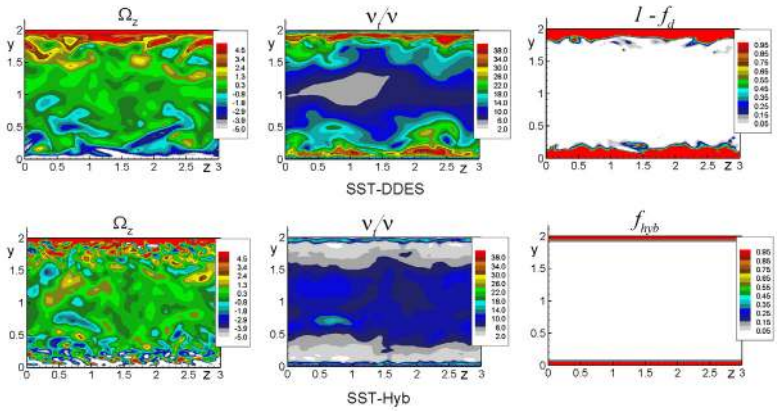

Figure 8: Comparison of *YZ*-cuts of instantaneous vorticity magnitude, eddy viscosity, and hybrid function from the simulation of the developed channel flow with the MSST-based version of the hybrid model (5) and MSST-based DDES at Re_τ=2400

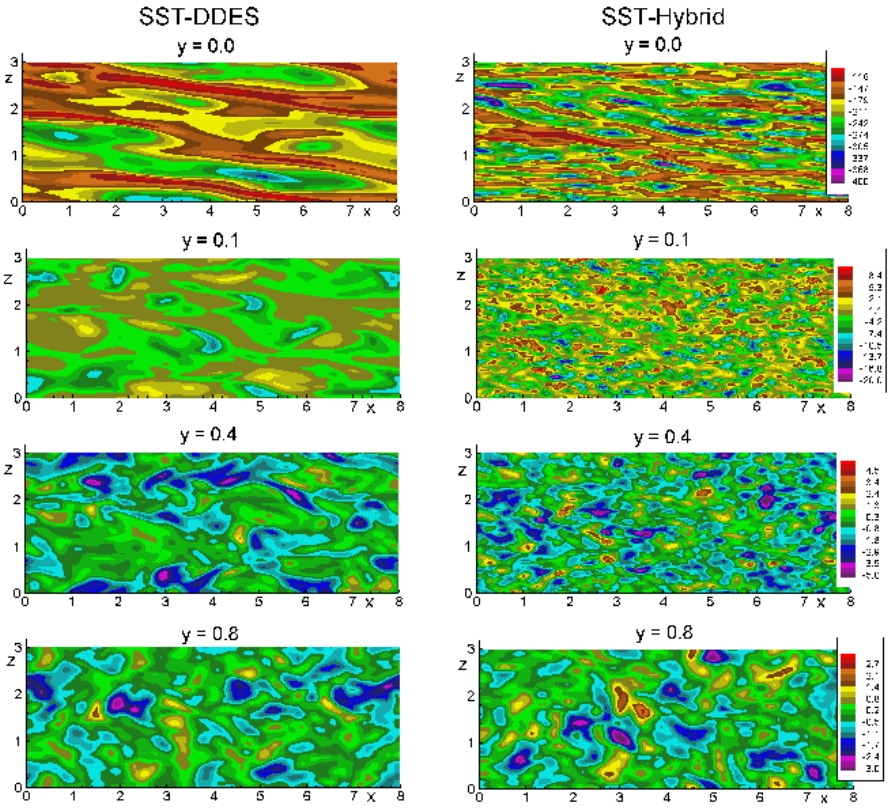

Figure 9: Comparison of *XZ*-cuts of instantaneous vorticity magnitude from the simulation of channel flow with the MSST-based version of the hybrid model (5) and MSST-based DDES at Re_τ=2400

Finally, the fields of the hybrid function shown in Figs.6, 8 are consistent with its profiles presented in Fig.4. In particular, they confirm that at Re_τ=400 the switch from RANS to LES mode is controlled solely by the function f_{step} and so depends only on the grid (the

RANS-LES interface is straight), while at Re_τ=18000, the solution-dependent $(1-f_d)$ branch of the hybrid function is also active (the interface is wavy).

A quantitative assessment of the MSST-based hybrid model performance can be done based on Fig.10, where we present the mean velocity profiles and resolved and modelled parts of the Reynolds stresses at different Re_τ predicted by this model. The velocity profiles are compared with the Reichardt correlation[21)]

$$U^+ = \frac{1}{\kappa}\ln(1.0+0.4y^+) + 7.8\left[1-\exp\left(\frac{y^+}{11}\right)-\left(\frac{y^+}{11}\right)\exp\left(-\frac{y^+}{3}\right)\right], \qquad (14)$$

which achieves fairly good agreement with the DNS data[18)] and so may be used as a benchmark. Note that the hybrid model performs well not only at the large Re_τ, which is arguably an easier case for WMLES[17)], but also at moderate and even low (corresponding to well-resolved LES) Re_τ.

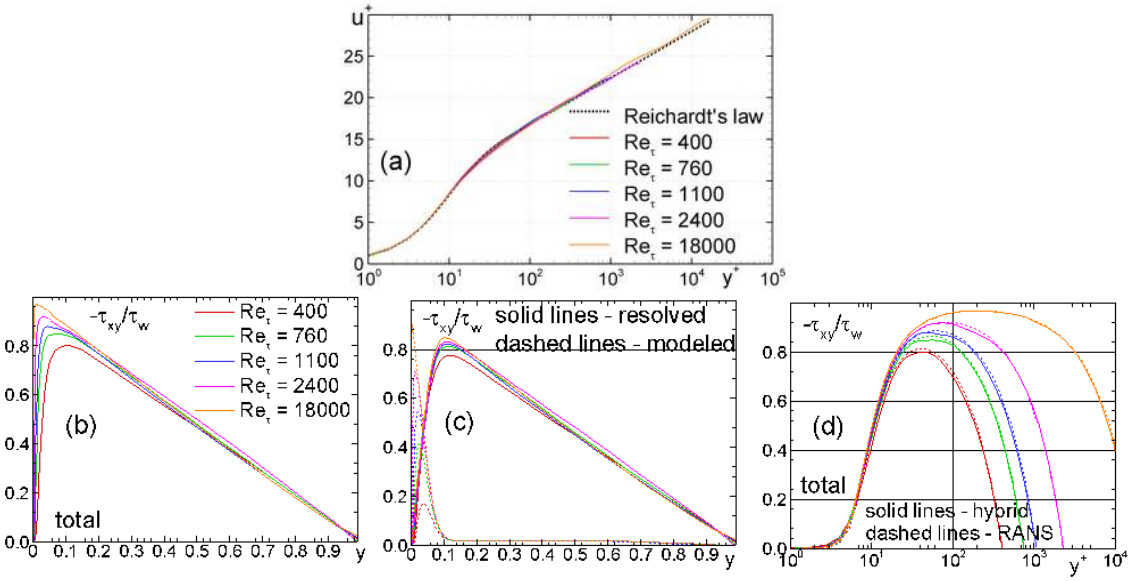

Figure 10: Profiles of mean velocity (a), total (b) and resolved and modeled shear stresses (c) from the simulations of d channel flow at different Re_τ with the use of MSST-based version of the hybrid model (5) and comparison of the total shear stresses predicted by this model with those of MSST RANS (d)

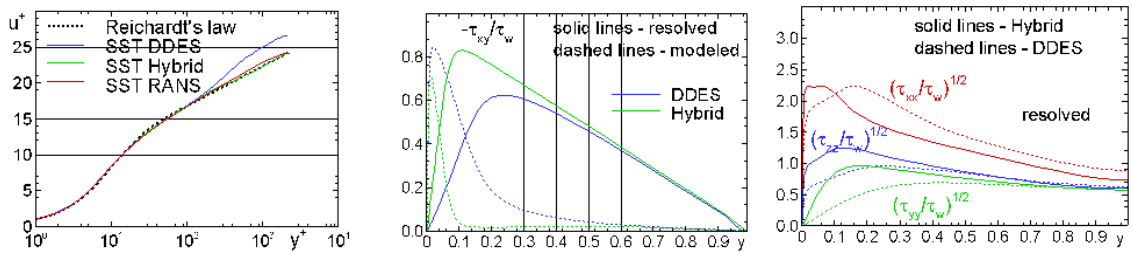

Figure 11: Comparison of predictions of channel flow at Re_τ=2400 provided by the MSST-based version of the hybrid model (5) and MSST-based DDES

Finally, Fig.11 presents a direct comparison of the mean flow velocity and Reynolds stresses predicted by the MSST-based version of the hybrid model (5) with MSST-based DDES at Re_τ=2400. It shows that the hybrid model leads to a significant increase of the resolved part of the stress, and to a complete elimination of the LLM typical of DES97 and DDES.

To conclude the discussion of simulations of channel flow with the use of the MSST-based version of the hybrid model (5) operating in WMLES mode, it should be noted that all the results presented above were obtained on grids with the streamwise step, Δx, twice as large as the spanwise step, Δz. Although this is common LES practice motivated by the knowledge of the turbulence structure in the channel, it is of interest to evaluate the reaction of the model to an alteration of the $\Delta x/\Delta z$ value. It is illustrated by Fig.12, where the results of the simulations at $\Delta x/\Delta z$=2 are compared with those at $\Delta x/\Delta z$=1 and 4, Δz being kept constant. The value 1 is much more likely in engineering practice, since the direction of the flow, especially very near the wall, is not known at the grid-design stage. One can see that, as expected, an increase of $\Delta x/\Delta z$ results in a growth of the modelled and decrease of the resolved parts of the shear stresses. However, in the considered range of $\Delta x/\Delta z$ this does not cause a significant alteration of the total shear stress and the mean velocity profile. Therefore, the dependence chosen on Δx and Δz individually appears quite successful.

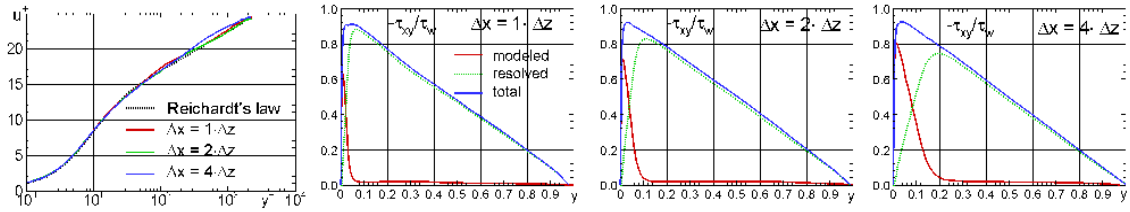

Figure 12: Effect of streamwise grid step on prediction of developed channel flow at Re_τ =2400 provided by MSST-based version of the hybrid model (5)

Let us now consider the model performance in the case without initial turbulent content. This situation has been implemented by starting the simulations from a steady MSST RANS solution. In this case, independently of the Reynolds number, the solution returned by the hybrid model is identical to the initial RANS solution, which is exactly what was expected. Indeed, as seen in Fig.13, in this case, one of the two functions defining $f_{restore}$ (either f_l or f_t) is equal to 1.0, which results in the zeroing of f_{amp} (see (11)) and, therefore, of $f_{restore}$ as well (see (9)). Considering that the hybrid function computed by the RANS solution is equal to (1- f_d), this means that the hybrid model effectively performs as DDES does in this situation, i.e., results in the RANS solution[5]. This is also seen in Fig.13, where the velocity profiles obtained with the use of the hybrid model are plotted by dashed lines. Recall that this preservation of RANS was introduced in DDES in order to avoid the inaccuracies that result from the activation of the DES limiter in grids that are not fine enough to support a quality LES.

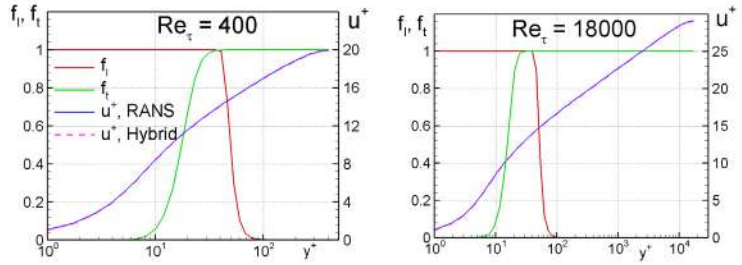

Figure 13: Profiles of the functions f_t and f_l defined by (12) and mean velocity in the channel computed with the use of MSST-based version of the hybrid model (5) initialised by the SST-RANS solution (dashed line)

SA-based version of the hybrid model. In general, the performance of this version of the hybrid model (5) is quite similar to that of the MSST-based counterpart considered above. The only difference between these two versions is that with MSST, the function Ψ is equal to 1.0, while for the SA it is defined by the relation (14). As already mentioned, the function expresses the so-called low-Reynolds number correction aimed at compensating the non-justified activation of the low-Re number terms of the SA RANS model in the LES mode of the SA-based DES (the need for its introduction and the derivation of the correction (14) are discussed in detail in[5]). However the introduction of the same function in the RANS branch of the hybrid model, as done in the present work (see relation (5)), is purely empirical, and a better function could probably be suggested for this purpose. Nonetheless, even with this function, the model performance turns out quite satisfactory, so that a search for another function does not seem to be crucial. This is supported by Fig.14, where we present profiles of the quantity $f_{restore}\Psi$ involved in the formulation of the model (5) and show plots of the profiles of the ratio of the hybrid and RANS turbulent lengths-scales $\tilde{l}/d_w$ across the channel. One can see that qualitatively the variation of these functions across the channel is similar to that observed for the corresponding functions in the MSST-based version of the hybrid model. The only difference is that at the lower Reynolds numbers, the SA-based version needs more "assistance" in the RANS region than the MSST-based version does (compare Fig.14 with Fig.5).

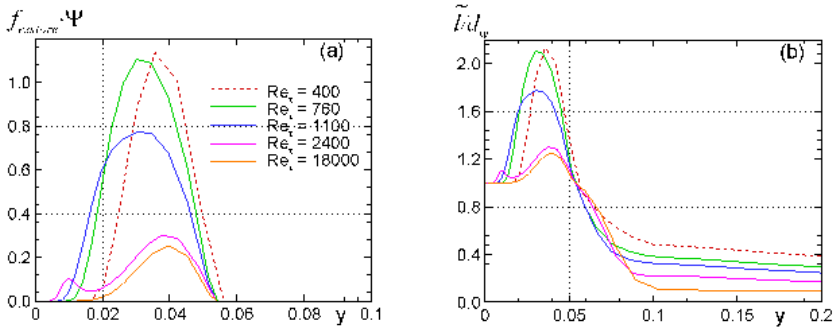

Figure 14: Profiles of the quantity $f_{restore}\Psi$ (a) and ratio of length-scales of SA-based version of the hybrid model (5) and SA RANS model (b) in channel flow

As a result, the performance of the SA-based version of the hybrid model in WMLES mode, i.e., in the case of the simulations with turbulent content (initialised by the DIHT LES solution) turns out to be virtually the same as that of the MSST model considered above. This is seen in Fig.15, where we present the mean velocity profiles and shear stresses from the simulations of the channel flow at different Re_τ carried out with the use of this model. This weak dependence is viewed as a strength for DES.

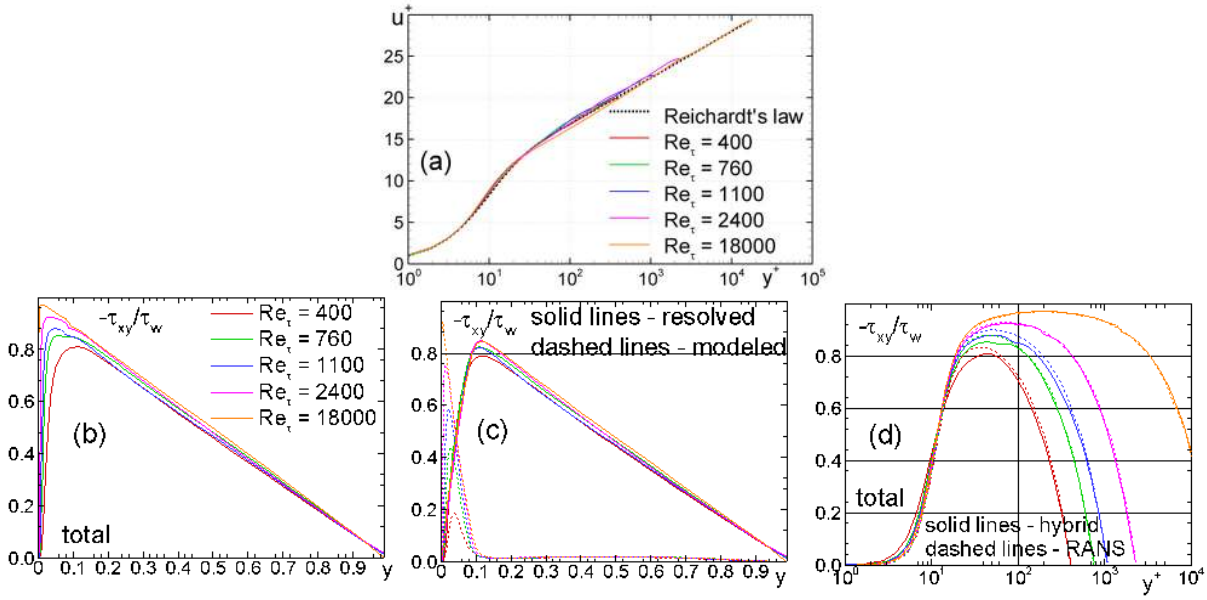

Figure 15: Profiles of mean velocity (a), total (b) and resolved and modeled shear stresses (c) from the simulations of channel flow at different Re_τ with the use of SA-based version of the hybrid model (5) and comparison of the total shear stresses predicted by this model with those of SA RANS (d)

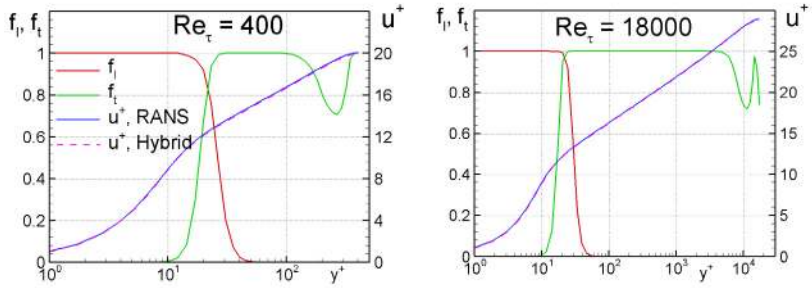

Figure 16: Profiles of the functions f_t and f_l defined by (10) and mean velocity in the channel computed with the use of SA-based version of the hybrid model (5) initialised by the SA-RANS solution (dashed line)

As for the case without turbulent content, due to the non-perfection of the function Ψ in the RANS branch of the model mentioned above, the performance of the SA-based hybrid model turns out to be a bit worse than that of the MSST-based model. The reason is clear in Fig.16, where we present plots of the functions f_l and f_t which define the amplitude of the

restoring function f_{amp}. The figure shows that there is a region where both f_l and f_t deviate from the value of 1.0, which results in a non-zero $f_{restore}$ and, consequently, in some deviation of the solution provided by the hybrid model from that of the background SA RANS model. However, as also seen in Fig.16, this deviation is very weak.

Thus, summarising, we can conclude that both versions of the hybrid model (5) have passed the channel-flow test equally well.

3.4 Backward-facing step flow

This flow is a rather severe test for the new model, since in this case it must automatically provide three different types of behaviour depending on the flow region. Namely, it should function as a RANS model in the attached boundary layers upstream of the step and on the upper wall of the channel which do not have any "turbulent content", as LES in the separation zone, and, finally, as WMLES in the reattached boundary layer on the step-wall, which inherits a "turbulent content" from the upstream separation zone.

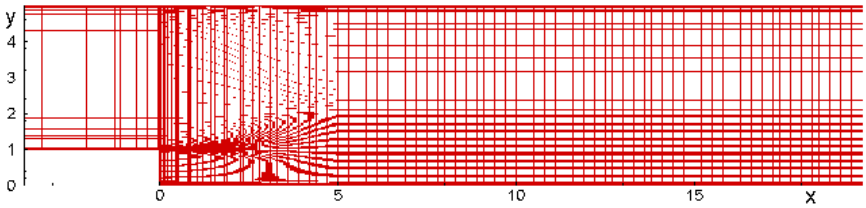

Figure 17: Computational grid in *XY* plane of BFS flow of Vogel and Eaton[13)]

As mentioned in Section 3.1, the specific flow we have considered is that studied experimentally by Vogel and Eaton[13)]. It is a flow in a plane channel with the step on the lower wall. The Reynolds number based on the step height, *H*, is equal to 28,000 and the channel expansion ratio is 5/4. The incoming boundary-layer thickness is 1.07*H*. The computational domain and the *XY*-plane grid used in the simulations are shown in Fig.17. The grid contains 1.5 million nodes. It is uniform in the spanwise direction (the span size of the domain is equal to 2 step heights, and the non-dimensional step Δz is equal 1/30).

Results of the simulations suggest that both the SA- and MSST-based versions of the hybrid model (5) satisfy the demands formulated above. As an example, in the left column of Fig.18 we show *XY*-cuts of the instantaneous fields of vorticity magnitude, eddy viscosity, and hybrid function and then a snapshot of vorticity on the lower wall of the channel downstream of the step from the simulation with the use of the MSST-based version of the model. It shows, in particular, that in the attached boundary layers approaching the step and in the boundary layer at the upper wall, the $(1-f_d)$ branch of the models is active, while at the step-side the f_{step} branch prevails (results of the simulation with the use of the SA-based hybrid model (not shown) are virtually the same). Moreover, a comparison of the results obtained with the use of the MSST-based hybrid model with those predicted by the MSST DDES (right column in Fig.18) reveals noticeable advantages for the new model. In

particular, in the vicinity of the step-wall, where the hybrid model operates in the WMLES mode, it returns a lower level of eddy viscosity than that of DDES operating in RANS mode. As a result, the hybrid model provides a better resolution of the fine turbulent structures, which is especially important for the region of recovery of the reattached boundary layer, which remains the most challenging for both RANS and DDES. This leads to a more accurate prediction of the mean flow characteristics by both SA- and MSST-based versions of the hybrid model not only versus the corresponding background RANS models but, what is more important, versus the corresponding DDES versions as well.

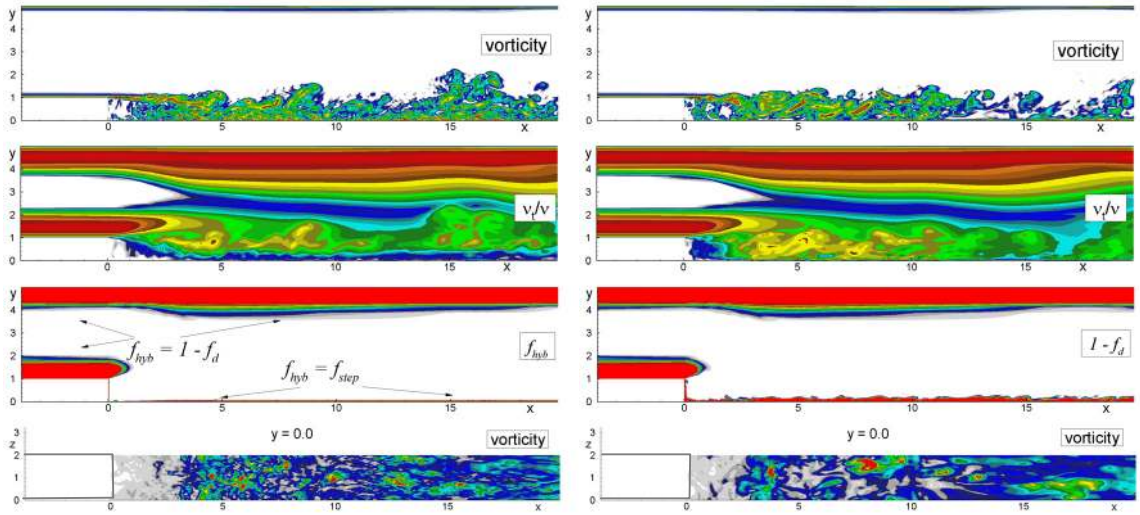

Figure 18: *XY*-cuts of the instantaneous fields of vorticity magnitude, eddy viscosity and hybrid function, and snapshots of the vorticity magnitude on the step wall from simulations of Vogel & Eaton BFS flow[13] with the use of MSST-based hybrid model (left) and MSST-based DDES (right)

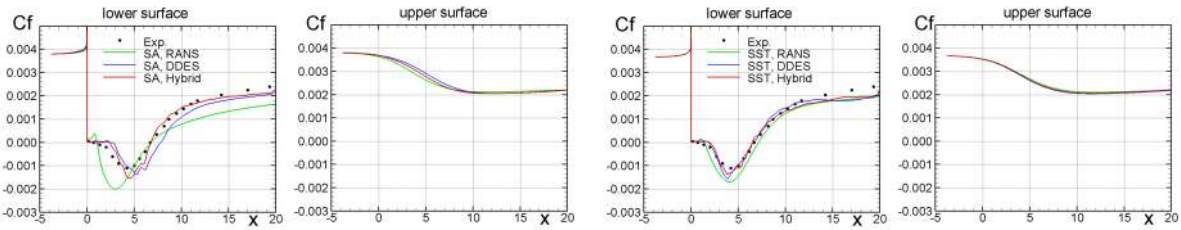

Figure 19: Comparison of the mean friction coefficient distributions in the BFS flow predicted by RANS, DDES and hybrid models with the data of Vogel & Eaton[13]

This is seen in Figs.19, 20, where we compare the skin friction distributions over the straight and step-walls of the channel and mean velocity profiles computed with all these models with the experimental data of Vogel & Eaton. Note that, consistently with the better representation of turbulence, the superiority of the new hybrid models over DDES shows up not only with regard to the prediction of the flow in the recirculation zone downstream of the step, but also in the region of flow recovery after reattachment. The skin friction remains under-predicted past $x = 12$, which appears like a failure to fully repair LLM; we speculate

that the spanwise domain ($2H$) may be too narrow, and also note that the flow is far from having settle again into a normal zero-pressure-gradient boundary layer. A finer grid may simply be needed for such a flow.

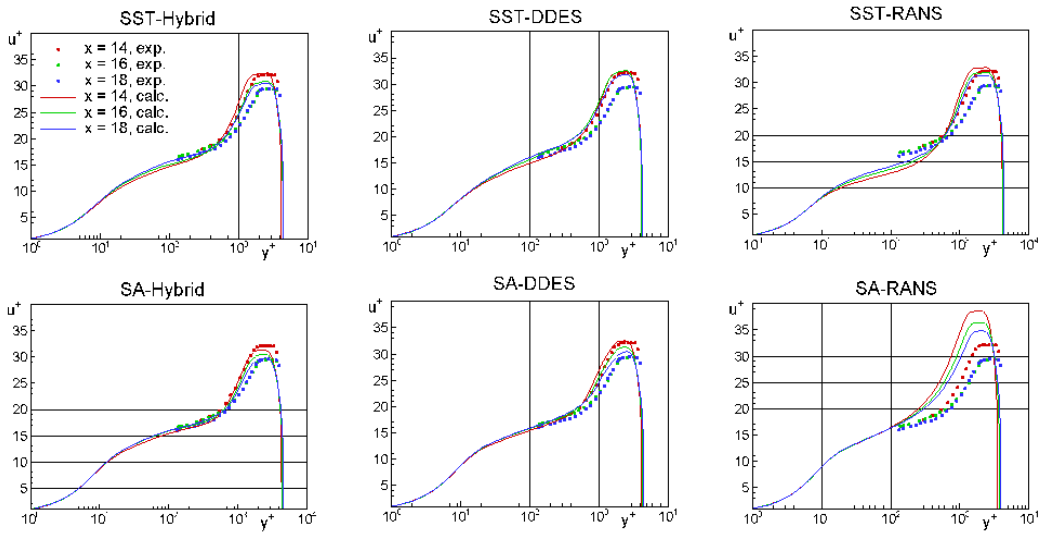

Figure 20: Comparison of the mean velocity profiles in the recovery region of the BFS flow predicted by RANS, DDES and hybrid models with the data of Vogel & Eaton[13)]

3.5 NACA0021 airfoil at 60 degrees angle of attack

The flow has been studied in experiments[14)] at Reynolds number Re_c=2.70×10^5, based on the free-stream velocity and the airfoil chord. Simulations are performed with the use of the SA-based versions of the hybrid model (5) and DDES and, also, with the original DES97 model. These run in fully turbulent mode; the inflow eddy viscosity is specified equal to the molecular viscosity, which leads to its immediate growth when fluid enters a boundary layer. The same grid is used in all the simulations. In the *XY*-planes it is of O-type and has 141×101 nodes in the streamwise and wall-normal directions respectively. The near-wall *y*-step is equal $5\times10^{-5}c$ (which provides y_1^+ less than 1.0) and rises with a stretching factor less than or equal to 1.3. The outer boundary of the domain is a circle with a radius of $15c$, and the span-size of the domain is $1c$, with periodic boundary condition. The spanwise grid is uniform with $\Delta z/c = 0.033$.

Figure 21 shows snapshots of the vorticity magnitude and hybrid function together with a fragment of the grid. It suggests that in this flow, just as in the BFS flow considered in the previous section, both branches of the hybrid function (6) are active. The $(1-f_d)$-branch prevails over the upper surface of the airfoil, where massive separation takes place, while the f_{step}-branch is active near the lower surface with attached flow and no turbulent content. As a result, consistently with the idea the hybrid model (5) is based on, the mean flow characteristics predicted by this model turn out to be very close to those obtained with DES97 and DDES. This is seen from a comparison of the mean pressure and friction coefficients

distributions computed with the use of all the considered models, presented in Fig.22 (a minor difference between the different curves is explained mostly by the different time samples in different simulations).

Thus, the test confirms that for massively separated flows, the hybrid model (5) performs quite the same as the original DES97 and DDES.

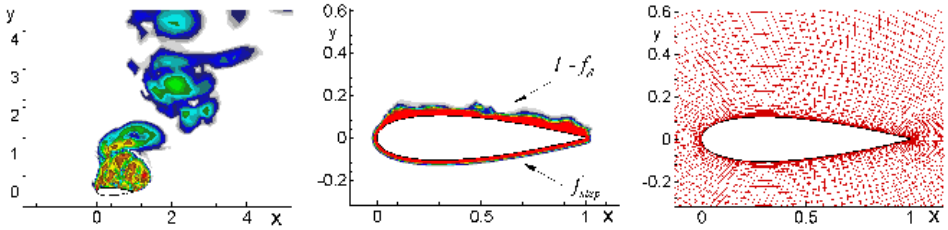

Figure 21: Snapshots of vorticity magnitude and hybrid function (6) and a fragment of the grid from simulation of NACA 0021 airfoil at 60° angle of attack with the use of SA-based version of the hybrid model (5)

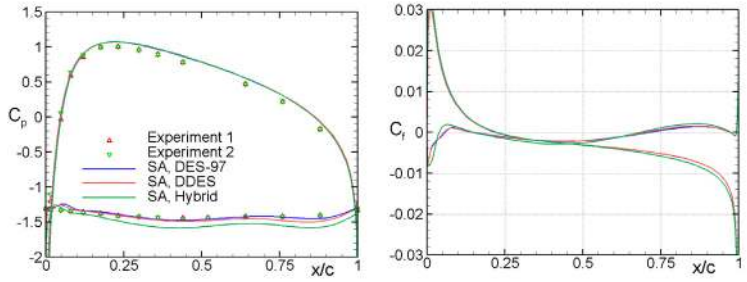

Figure 22: Mean pressure and friction coefficients distributions over NACA 0021 airfoil at 60° angle of attack predicted by the hybrid model (5), DES97, and DDES based on the SA RANS model. Symbols - experimental data[14] at two span-sections of the airfoil

4 CONCLUSIONS

The mismatch between the modeled log layer and the resolved log layer, discovered in 2000 when either DES97 or DDES is used for wall modeling in an LES, can be resolved by modifications which are relatively simple and cost-free, and appear robust based on the fair set of test cases presented here. Modifications have been presented for either DES97 or DDES, and either the S-A or the SST base RANS model. The method still works in its natural mode, aimed at external flows, and is more attractive for internal flows and other cases which justify activating LES inside the boundary layer. On the other hand, it has not been demonstrated for unstructured grids, and a higher degree of simplicity may be desired in such applications. However, Wall-Modeled LES on unstructured grids is far from common, if it has even been achieved at all. The behavior of the new versions also needs to be verified in grids that are not distributed as smoothly as the present ones, although the backward-facing step shown here does contains needlessly fine regions, linked to the structured character of the grid. In general, prudent modifications such as the one which creates DDES and the ones developed here appear to preserve and even broaden the basis of DES, namely the ability to activate RANS and LES in different flow regions, giving a well-balanced and powerful numerical approach to complex turbulent flows at high Reynolds numbers.

ACKNOWLEDGEMENTS

Authors from NTS were partially supported by the EC within the research project DESIDER under contract No. AST3-CT-200-502842 (http://cfd.me.umist.ac.uk/desider).

REFERENCES

[1] L. Davidson, S. Dahlstrom, "Hybrid LES-RANS: an approach to make LES applicable at high Reynolds number", *International Journal of Computational Fluid Dynamics*, **19**, No.6, 415–427 (2005).

[2] L. Davidson, M. Billson, "Hybrid LES-RANS using synthesized turbulence for forcing", In: Proceedings of European Congress on Computational Methods in Applied Sciences and Engineering ECCOMAS 2004, P. Neittaanmaki, T. Rossi, S. Korotov, E. Onate, J. Periaux, and D. Knorzer (eds.) Jyvaskyla, 24–28 July 2004.

[3] L. Temmerman, M. Hadziabdic, M.A. Leschziner, K. Hanjalic, "A hybrid two-layer URANS–LES approach for large eddy simulation at high Reynolds numbers", *International Journal of Heat and Fluid Flow*, **26,** 173–190, (2005).

[4] V. Nikitin, F. Nicoud, B. Wasistho, K.D. Squires, P.R. Spalart, "An Approach to Wall Modeling in Large-Eddy Simulations", *Physics of Fluids*, **12**, No.7, 1629-1632 (2000).

[5] P.R. Spalart, S. Deck, M.L. Shur, K.D. Squires, M.Kh. Strelets, A. Travin, "A new version of Detached-Eddy Simulation, resistant to ambiguous grid densities", Accepted for publication in *Theoretical and Computational Fluid Dynamics* (2006)

[6] P.R. Spalart, W.-H. Jou, M. Strelets, S.R. Allmaras, "Comments on the feasibility of LES for wings, and on a hybrid RANS/LES approach", First AFOSR International Conference on DNS/LES, Aug. 4-8 1997, Ruston, Louisiana.

[7] F.R. Menter, M. Kuntz, "Adaptation of eddy-viscosity turbulence models to unsteady separated flow behind vehicles". In: Proceedings of Symp. "The aerodynamics of heavy vehicles: trucks, buses and trains", Monterey, USA, Dec. 2002, R. McCallen, F. Browand & J. Ross, eds. Springer (2004).

[8] M. Shur, P.R. Spalart, M. Strelets, A. Travin: Detached-eddy simulation of an airfoil at high angle of attack", 4th Int. Symp. Eng. Turb. Modelling and Measurements (ETMM4), 669-678, Elsevier (1999).

[9] P.R. Spalart, "Strategies for turbulence modelling and simulations", *Int. J. Heat Fluid Flow*, **21**, 252-263 (2000).

[10] M. Strelets, "Detached Eddy Simulation of massively separated flows", *AIAA Paper,* AIAA-2001-879 (2001).

[11] P.R. Spalart, S. R. Allmaras, "A one-equation turbulence model for aerodynamic flows", *La Rech. Aerospatiale* No.1, 5-21 (1994).

[12] F.R. Menter, "Zonal two-equation k-ω turbulence models for aerodynamic flows", *AIAA Paper*, AIAA-93-2906 (1993).

[13] J.C. Vogel, J.K. Eaton, "Combined heat transfer and fluid dynamic measurements downstream of a backward-facing step", *J. Heat and Mass Transfer (Trans. ASME).* **107**, 922-929 (1985).

[14] K.E. Swalwell, "The Effect of Turbulence on Stall of Horizontal Axis Wind Turbines", Ph.D. Thesis, Department of Mechanical Engineering, Monash University (2005).
[15] S.E. Rogers, D. Kwak, "An upwind differencing scheme for the time-accurate incompressible Navier-Stokes equations", *AIAA Paper*, AIAA 88-2583-CP (1988).
[16] A. Travin, M. Shur, M. Strelets, and P.R. Spalart, "Physical and numerical upgrades in the Detached-Eddy Simulation of complex turbulent flows", In: Fluid Mechanics and its Applications. *Advances in LES of Complex Flows*, R.Friederich and W.Rodi (editors). **65**, 239-254 (2002). Proc. of EUROMECH Colloquium 412, Kluwer Academic Publishers, Dordrecht / Boston/ London.
[17] U. Piomelli, P. Moin, J.H. Ferziger, "Model consistency in Large-Eddy Simulation of turbulent channel flows", *Physics of Fluids*, **31**, 1884-1894 (1988).
[18] R.D. Moser, J. Kim, and N.N. Mansour, "DNS of turbulent channel flow up to Re_τ=590", *Physics of Fluids,* **11**, 943-945 (1999).
[19] P.R. Spalart, M. Strelets, A. Travin, "Direct Numerical Simulation of Large-Eddy-Break-Up Devices in a Boundary Layer", In: Int. Symp. Eng. Turb. Modelling and Measurements VI, May 2005, Sardinia. W. Rodi, ed.
[20] U. Piomelli and E. Balaras, "Wall-layer models for Large-Eddy Simulations", *Annu. Rev. Fluid Mech*., **4**, 349–74 (2002).
[21] H. Reichardt, "Vollstandige darstellung der turbulenten geschwindigkeitsverteilung in glatten leitungen", *Zeitschrift für Angewandte Mathematik und Mechanik*, **31**, 208-219, (1951).